

Supporting Information

Confined Sub-nanometer PtCo Cluster as a Highly Efficient and Robust Electrocatalyst for Hydrogen Evolution Reaction

Fei Guo ^a, Zhijin Zou ^a, Zeyi Zhang ^a, Tang Zeng ^a, Yangyang Tan ^a, Runzhe Chen ^a, Wei Wu ^a, Niancai Cheng ^{*a} and Xueliang Sun ^{*b}

^a College of Materials Science and Engineering, Fuzhou University, Fuzhou, 350108
China.

^b Department of Mechanical and Materials Engineering, University of Western Ontario,
London, ON N6A 5B9, Canada.

*Corresponding author

Niancai Cheng, E-mail: niancaicheng@fzu.edu.cn; orcid.org/0000-0002-6358-5515.

Xueliang Sun, E-mail: xsun@eng.uwo.ca; orcid.org/0000-0003-0374-1245.

Experimental section

Reagents. All the chemicals used were commercial without any further purification. Zinc nitrate hexahydrate ($\text{Zn}(\text{NO}_3)_2 \cdot 6\text{H}_2\text{O}$; >99.0%, Sinopharm Chemical Reagent Co., Ltd.), 2-methyleimidazole (99.0%, Aladdin), methanol (99.5%, Sinopharm Chemical Reagent Co., Ltd.), Cobalt nitrate hexahydrate ($\text{Co}(\text{NO}_3)_2 \cdot 6\text{H}_2\text{O}$; >99.0%, Sinopharm Chemical Reagent Co., Ltd.), ethanol (99.5%, Sinopharm Chemical Reagent Co., Ltd.), Hexachloroplatinum (IV) acid ($\text{H}_2\text{PtCl}_6 \cdot 6\text{H}_2\text{O}$; >37.5%, Sinopharm Chemical Reagent Co., Ltd.), Pt/C (Johnson Matthey, 20%), sulfuric acid (95%, Sinopharm Chemical Reagent Co., Ltd.) and de-ionized water with the specific resistance of $18.25 \text{ M}\Omega \cdot \text{cm}^{-1}$ (obtained by reversed osmosis followed by ion-exchange and filtration).

Synthesis of NPC. The ZIF-8 was synthesized according to a reported procedure. The prepared ZIF-8 was grinded into a powder and transferred into a quartz tube and then heated at 1000°C for 2h under N_2 atmosphere. The obtained black powder was named NPC.

Synthesis of Co/NPC. The $\text{Co}(\text{NO}_3)_2 \cdot 6\text{H}_2\text{O}$ (50 mg) was dissolved in the 50ml ethanol with stirring, then the prepared NPC (100 mg) was added to the solutions with ultrasonic stirring for four hours, the samples were acquired by centrifugation and washed by ethanol. After drying overnight, the samples were transferred to a quartz tube and heat-treated at 500°C for 1h in a hydrogen atmosphere. The obtained samples were recorded as Co/NPC.

Synthesis of PtCo/NPC. The $\text{H}_2\text{PtCl}_6 \cdot 6\text{H}_2\text{O}$ (5.4 mg, 14.0 mg, 29.5 mg) was dissolved in 50ml ethanol, then the prepared Co/NPC (100 mg) was added into the solutions with

ultrasonic stirring for four hours, the samples were acquired by centrifugation and washed by ethanol. After drying overnight, the samples were transferred to a quartz tube and heat-treated at 500°C for 1h in a hydrogen atmosphere. The Pt loading on these samples were 1.2, 2.5, 6.5wt%, respectively, by ICP. The obtained samples were recorded as 1.2%PtCo/NPC, 2.5%PtCo/NPC and 6.5%PtCo/NPC, respectively.

Synthesis of Pt/NPC. The $\text{H}_2\text{PtCl}_6 \cdot 6\text{H}_2\text{O}$ (5.4 mg) was dissolved in 50ml ethanol, then the prepared NPC (100 mg) was added into the solution with ultrasonic stirring for four hours, the sample was acquired by centrifugation and washed by ethanol. After drying overnight, the sample was transferred to a quartz tube and heat-treated at 500°C for 1h in a hydrogen atmosphere. The Pt loading is 1.3% according to the ICP testing. The obtained sample was recorded as 1.3%Pt/NPC.

Material characterization. Scanning electron microscopy (SEM) was performed on a SUPRA 55. Transmission electron microscopy (TEM) images and Wide-angle X-ray diffraction (XRD, D-MAX 2200 VPC) patterns. X-ray photoelectron spectroscopy (XPS) characterization was performed by a K-Alpha. Inductively coupled plasma mass spectrometer (ICP-MS) (iCAP7000, Thermo Fisher Scientific) was used to determine the Pt loading. The particle size distribution was determined by measuring more than 200 particles using a Nano Measurer.

Electrochemical methods. All the electrochemical measurements were conducted in a three-compartment cell at room temperature on an electrochemical workstation

(CHI660E). The carbon rod and Ag/AgCl electrode were utilized as the counter and reference electrodes, respectively. The working electrode was as-prepared catalysts coated with a glassy carbon electrode. The electrolyte was N₂ saturated 0.5 M H₂SO₄. The catalyst ink was prepared by blending the catalyst powder (2 mg) with 20 uL Nafion solution (5 wt%) and 980 uL of isopropanol in an ultrasonic bath. The catalyst ink was then pipetted onto the glassy carbon electrode surface (0.196 cm²). The potentials in this work were converted to RHE according to $E_{(RHE)} = E_{(Ag/AgCl)} + 0.197 + 0.059 \cdot pH$. Before measurements, a steady CV of the working electrode was first obtained by cycling at 0.05-1.2 V (vs. RHE) at 50 mV·s⁻¹ in a N₂-saturated 0.5 M H₂SO₄ solution. The hydrogen evolution reaction (HER) linear sweep voltammetry (LSV, 2 mV·s⁻¹) was performed in a N₂-saturated 0.5 M H₂SO₄. Note that all the HER LSV tests were 100% iR-compensated. The accelerated durability test (ADT) was performed by sweeping electrode between -0.15-0.25 V at 100mV/s for 1000 cycles in a N₂-saturated 0.5 M H₂SO₄. The Tafel slopes were calculated by fitting to the Tafel equation: $\eta = b \cdot \log j + c$. The TOF values were calculated based on the Pt atom numbers in each sample electrode according to the following equation: $TOF = \frac{I}{2F \cdot n}$, where I (in Amperes) is the current measured from LSV curves, F is the Faraday constant (96485.3, in C mol⁻¹) and n represents the atom number of Pt (in mol).

Density functional theory (DFT) calculation. All calculations are performed within the DFT framework, using the Vienna ab initio simulation package (VASP) that takes spin

polarization into account. We use the projected augmented wave (PAW) potentials to simulate the interaction between valence electrons and nuclei. In addition, Perdew-Burke-Ernzerh (PBE) and Generalized Gradient Approximation (GGA) using exchange correlation functions are used to study electron transfer and interrelationships. It is appropriate to select the kinetic energy cut-off point of plane wave expansion at 450 eV and the $3 \times 3 \times 1$ Monkhorst-Pack k-point grid sampling of the first Brillouin zone. To determine the occupancy, we set the Gaussian dispersion width to 0.1 eV. The relaxation of the adsorption surface structure was calculated using a conjugate gradient algorithm. The unit lattice constant was $14.793 \text{ \AA} \times 14.772 \text{ \AA} \times 30.000 \text{ \AA}$, and the maximum force and energy of unconstrained atoms were limited to 0.01 eV/\AA and $1 \times 10^{-6} \text{ eV}$, respectively. The electron iteration convergence value for self-consistent field (SCF) calculation was set to $1 \times 10^{-6} \text{ eV}$.

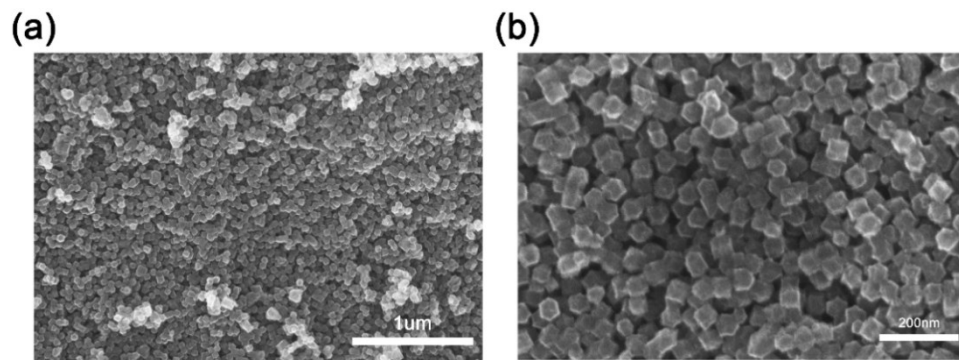


Fig. S1 SEM image of NPC.

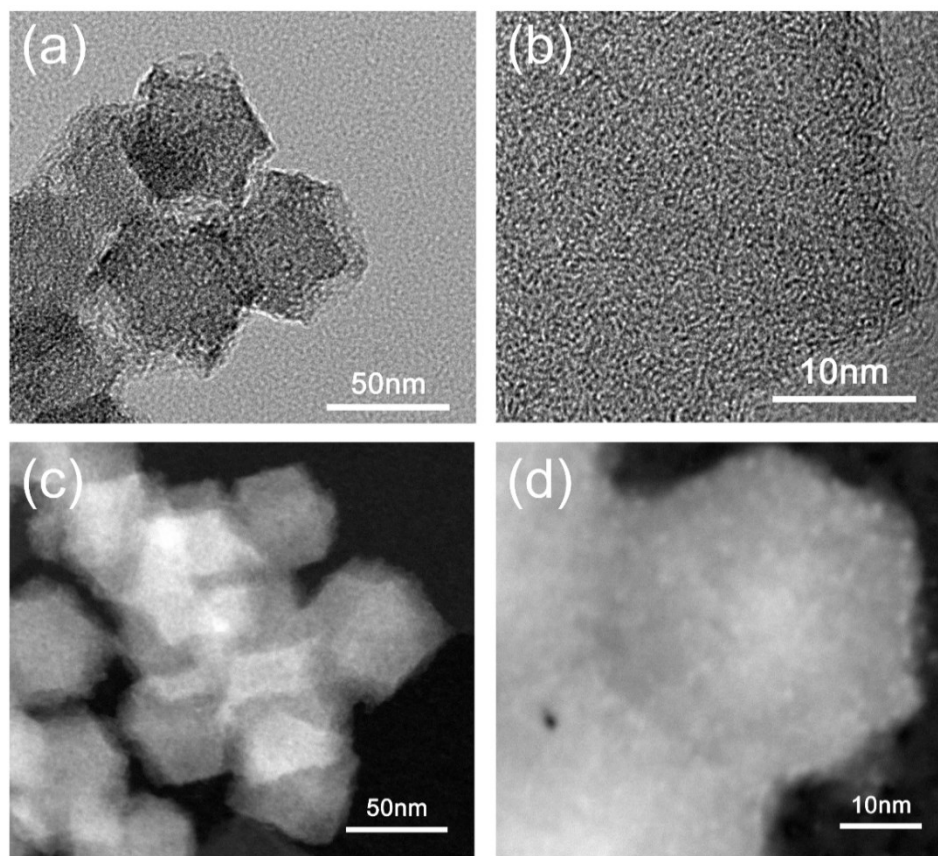


Fig. S2 (a-b) Bright-field TEM and HRTEM images of Co/NPC, (c-d) HAADF-STEM images of Co/NPC.

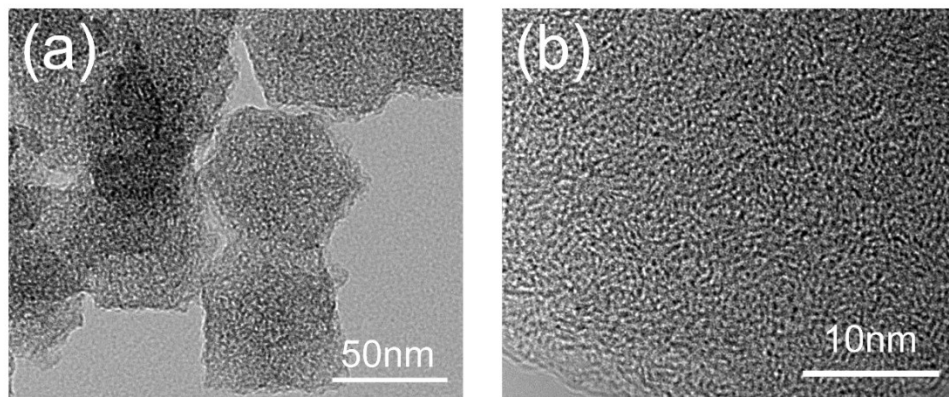


Fig. S3 Bright-field TEM and HRTEM images of 1.2%PtCo/NPC.

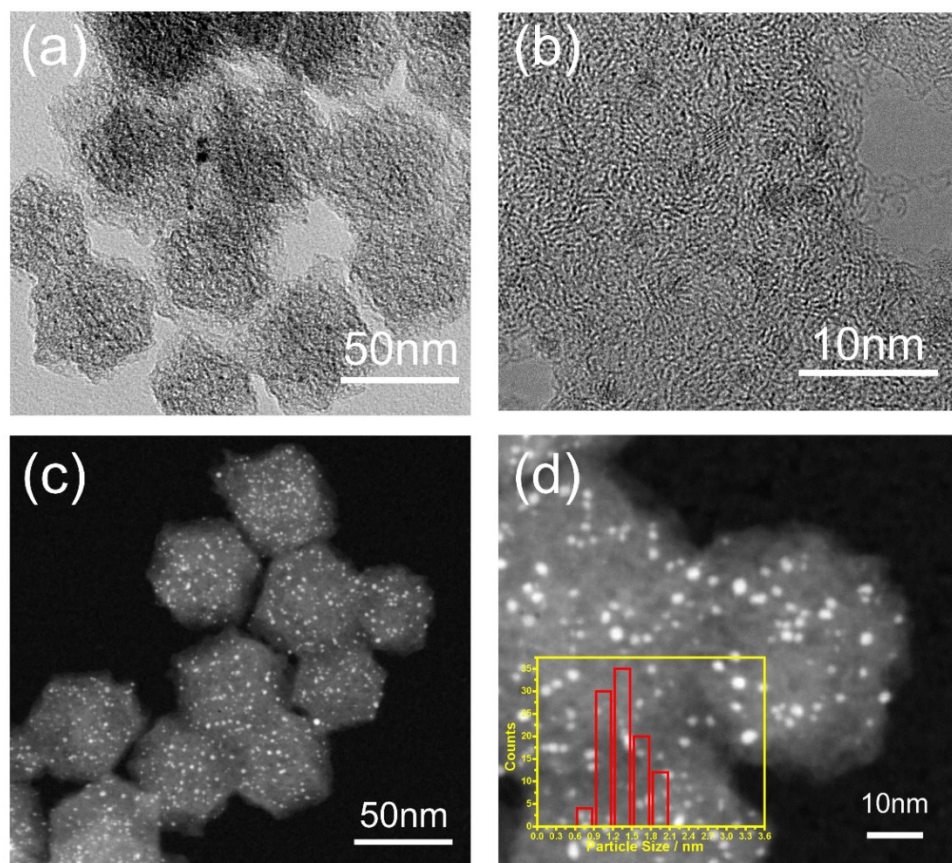


Fig. S4 (a-b) Bright-field TEM and HRTEM images of 2.5%PtCo/NPC, (c-d) HAADF-STEM images of 2.5%PtCo/NPC.

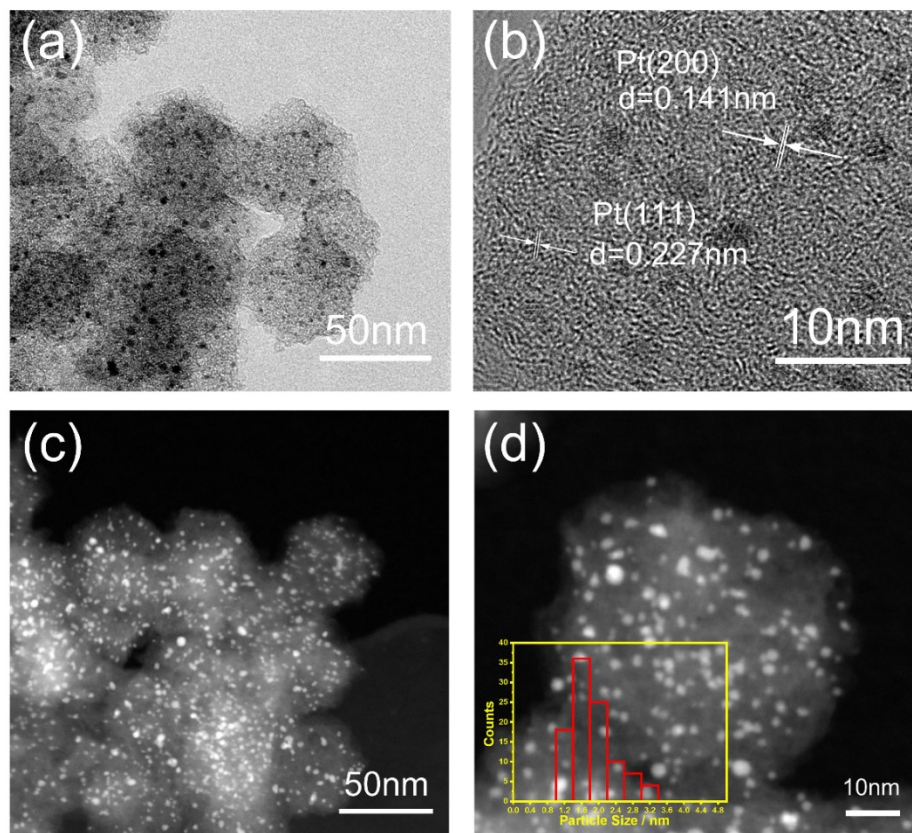


Fig. S5 (a-b) Bright-field TEM and HRTEM images of 6.5%PtCo/NPC, (c-d) HAADF-STEM images of 6.5%PtCo/NPC.

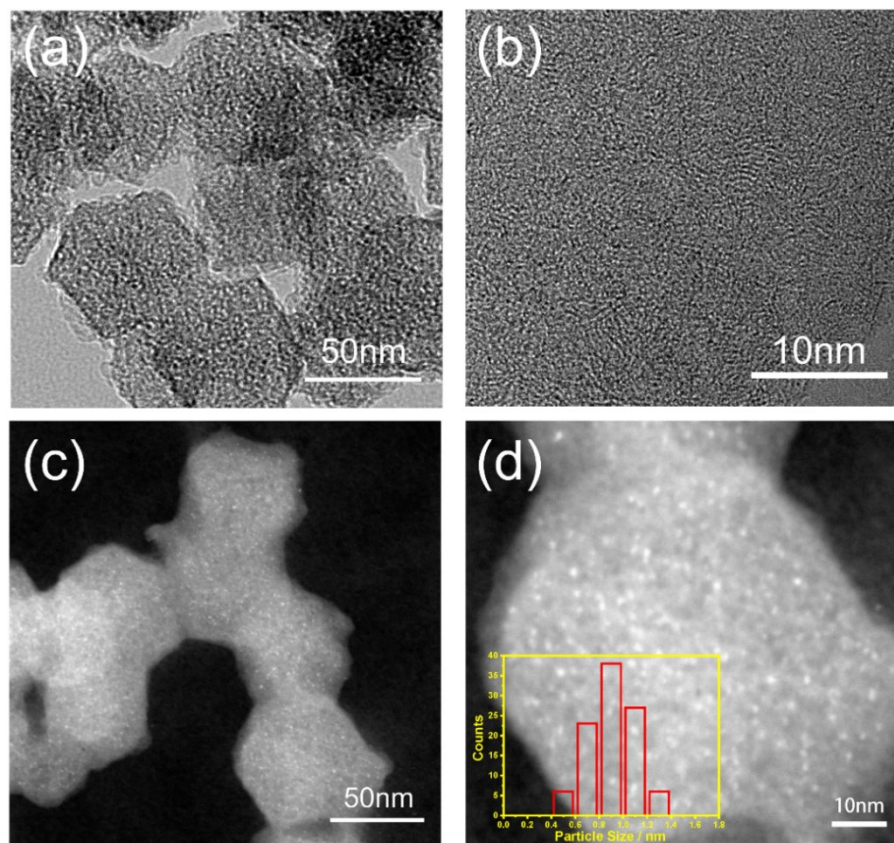


Fig. S6 (a-b) Bright-field TEM and HRTEM images of 1.3%Pt/NPC, (c-d) HAADF-STEM images of 1.3%Pt/NPC.

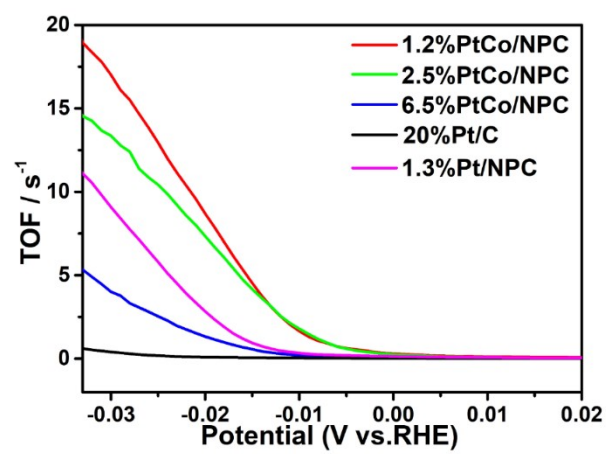


Fig. S7 TOFs of PtCo/NPC and commercial 20%Pt/C.

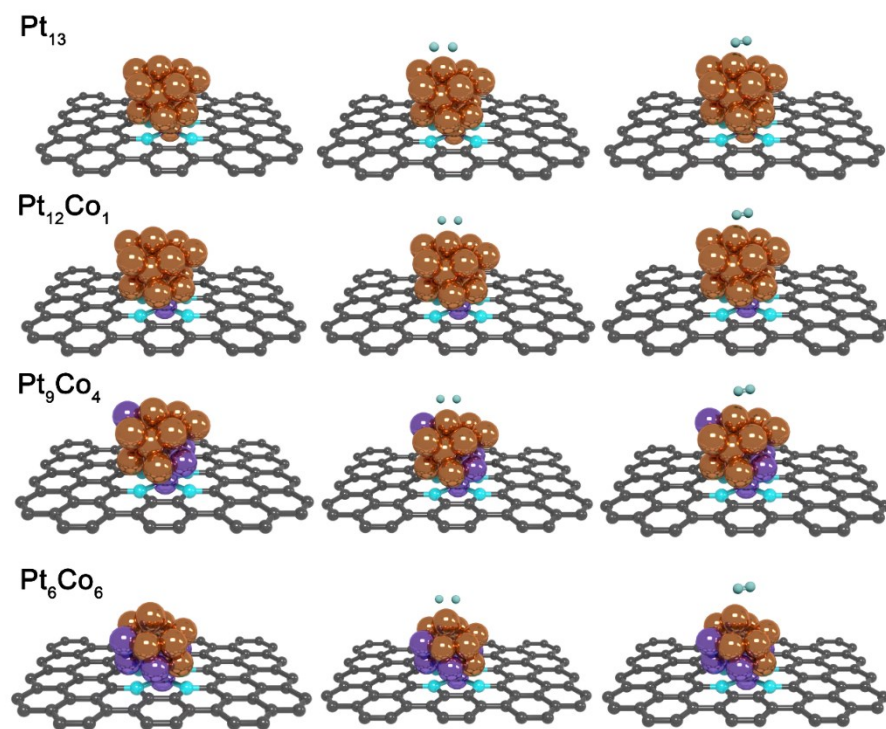


Fig. S8 The detailed structures for hydrogen adsorption and desorption on the surface of different models.

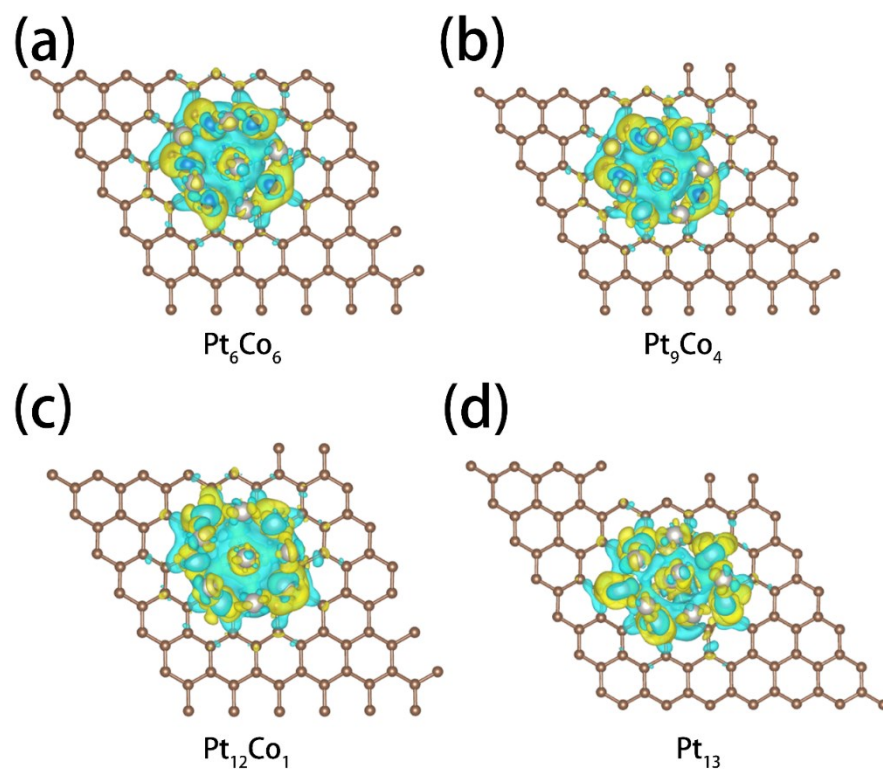


Fig. S9 The electron density difference in Pt_6Co_6 , Pt_9Co_4 , $\text{Pt}_{12}\text{Co}_1$ and Pt_{13} , where blue and yellow represent areas of electron diminishing and accumulation respectively.

Table S1. ICP-OES of Pt and Co mass percentage of different catalysts.

Samples	Pt	Co
Co/NPC	/	3.8
1.3%Pt/NPC	1.3	/
1.2%PtCo/NPC	1.2	0.39
2.5%PtCo/NPC	2.5	0.31
6.5%PtCo/NPC	6.5	0.15

Table S2. Cluster size statistics for PtCo/NPC.

Samples	Average cluster size (nm)
1.3%Pt/NPC	0.9
1.2%PtCo/NPC	0.8
2.5%PtCo/NPC	1.4
6.5%PtCo/NPC	2.0

Table S3. XPS spectra of different catalysts with Pt 4f.

Samples	Pt⁰4f_{7/2}	Pt²⁺4f_{7/2}	Pt⁰4f_{5/2}	Pt²⁺4f_{5/2}
1.3%Pt/NPC	71.17	72.08	74.24	75.47
1.2%PtCo/NPC	71.46	72.35	74.53	75.74
2.5%PtCo/NPC	71.38	72.29	74.45	75.68
6.5%PtCo/NPC	71.26	72.26	74.33	75.65

Table S4. XPS spectra of different catalysts with Co 2p.

Samples	Co 2p_{3/2}
Co/NPC	780.76
1.2%PtCo/NPC	780.36
2.5%PtCo/NPC	780.4
6.5%PtCo/NPC	780.61

Table S5. Comparison of the HER activity of the catalysts obtained in this work and other high-performance HER catalysts.

Catalyst	Overpotential at 10 mA·cm⁻²(mV)	Tafel slope (mV·dec⁻¹)	Mass activity (A mg⁻¹)	Ref.
1.2%Pt-Co/NC	14	21.2	13.83	This work
2.5%Pt-Co/NC	15	24.4	7.52	This work
6.5%Pt-Co/NC	20	26.9	1.34	This work
1.3%Pt /NC	19	25.5	5.86	This work
Pt/Co ₃ O ₄	70	33.5	0.02	1 ¹
Pt-T/G-150	30	30	6.84	2 ²
Pt ₁ /OLC	38	36	7.40	3 ³
Pd-Cu/Pt	175	58	3.00	4 ⁴
PtCu NSs/C	26.8	28.4	1.08	5 ⁵
Pt/RuCeO _x -PA	41	31	0.38	6 ⁶
Pt/GNs	25	33	2.24	7 ⁷
Pt/NPC	21.7	36.3	3.50	8 ⁸
Pt/def-WO ₃ @CFC	42	61	0.32	9 ⁹
Ni-MOF@Pt	43	30	0.13	10 ¹⁰
Pt-TiN NTAs	71	46.4	2.84	11 ¹¹

Table S6. The EIS fitting parameters from equivalent circuits of PtCo/NPC and commercial 20%Pt/C.

Samples	R_s/Ω	R_{ct}/Ω
1.3%Pt/NPC	4.86	10.08
1.2%PtCo/NPC	4.92	5.08
2.5%PtCo/NPC	4.85	7.87
6.5%PtCo/NPC	4.87	10.20
20%Pt/C	4.85	10.82

Table S7. The values of intermediate state (H^{*}) generations of different models.

Samples	Free energy / eV
Pt ₆ Co ₆	-0.03
Pt ₉ Co ₄	-0.06
Pt ₁₂ Co ₁	-0.26
Pt ₁₃	-0.52

Table S8. The peak value of activation energies for HER in Heyrovsky-step and Tafel-step.

Step	Energy / eV
Heyrovsky	0.38
Tafel	0.27

Table S9. The activation bond lengths of the intermediate H^{*} on different Pt-based model surfaces.

Samples	H[*] band length / Å
Pt ₆ Co ₆	1.595
Pt ₉ Co ₄	1.591
Pt ₁₂ Co ₁	1.571
Pt ₁₃	1.567

1. R. Jana, C. Chowdhury, S. Malik and A. Datta, *ACS Appl. Energy Mater.*, 2019, **2**, 5613-5621.
2. J. Ji, Z. Li, C. Hu, Y. Sha, S. Li, X. Gao, S. Zhou, T. Qiu, C. Liu, X. Su, Y. Hou, Z. Lin, S. Zhou, M. Ling and C. Liang, *ACS Appl. Mater. Interfaces*, 2020, **12**, 40204-40212.
3. D. Liu, X. Li, S. Chen, H. Yan, C. Wang, C. Wu, Y. A. Haleem, S. Duan, J. Lu, B. Ge, P. M. Ajayan, Y. Luo, J. Jiang and L. Song, *Nat. Energy*, 2019, **4**, 512-518.
4. T. Chao, X. Luo, W. Chen, B. Jiang, J. Ge, Y. Lin, G. Wu, X. Wang, Y. Hu, Z. Zhuang, Y. Wu, X. Hong and Y. Li, *Angew. Chem., Int. Ed. Engl.*, 2017, **56**, 16047-16051.
5. W. Li, Z.-Y. Hu, Z. Zhang, P. Wei, J. Zhang, Z. Pu, J. Zhu, D. He, S. Mu and G. Van Tendeloo, *J. Catal.*, 2019, **375**, 164-170.
6. T. Liu, W. Gao, Q. Wang, M. Dou, Z. Zhang and F. Wang, *Angew. Chem., Int. Ed. Engl.*, 2020, DOI: 10.1002/anie.202009612.
7. X. Yan, H. Li, J. Sun, P. Liu, H. Zhang, B. Xu and J. Guo, *Carbon*, 2018, **137**, 405-410.
8. C. Wang, F. Hu, H. Yang, Y. Zhang, H. Lu and Q. Wang, *Nano Res.*, 2016, **10**, 238-246.
9. H. Tian, X. Cui, L. Zeng, L. Su, Y. Song and J. Shi, *J. Mater. Chem. A*, 2019, **7**, 6285-6293.
10. K. Rui, G. Zhao, M. Lao, P. Cui, X. Zheng, X. Zheng, J. Zhu, W. Huang, S. X. Dou and W. Sun, *Nano Lett.*, 2019, **19**, 8447-8453.
11. J. Zhao, Y. Zeng, J. Wang, Q. Xu, R. Chen, H. Ni and G. J. Cheng, *Nanoscale*, 2020, **12**, 15393-15401.